LAWRENCE
LIVERMORE
NATIONAL
LABORATORY

LLNL-CONF-407829

Simulating the ITER Plasma Startup Scenario in the DIII-D Tokamak

G.L. Jackson, T.A. Casper, T.C. Luce, D.A. Humphreys, J.R. Ferron, A.W. Hyatt, T.W. Petrie, W.P. West

October 15, 2008

22nd IAEA-FEC
Geneva, Switzerland
October 13, 2008 through October 18, 2008

Disclaimer

This document was prepared as an account of work sponsored by an agency of the United States government. Neither the United States government nor Lawrence Livermore National Security, LLC, nor any of their employees makes any warranty, expressed or implied, or assumes any legal liability or responsibility for the accuracy, completeness, or usefulness of any information, apparatus, product, or process disclosed, or represents that its use would not infringe privately owned rights. Reference herein to any specific commercial product, process, or service by trade name, trademark, manufacturer, or otherwise does not necessarily constitute or imply its endorsement, recommendation, or favoring by the United States government or Lawrence Livermore National Security, LLC. The views and opinions of authors expressed herein do not necessarily state or reflect those of the United States government or Lawrence Livermore National Security, LLC, and shall not be used for advertising or product endorsement purposes.

Simulating the ITER Plasma Startup Scenario in the DIII-D Tokamak

G.L. Jackson 1), T.A. Casper 2), T.C. Luce 1), D.A. Humphreys 1), J.R. Ferron 1), A.W. Hyatt 1), T.W. Petrie 1), and W.P. West 1)

1) General Atomics, P.O. Box 85608, San Diego, California 92186-5608, USA
2) Lawrence Livermore National Laboratory, Livermore, California 94550, USA

e-mail contact of main author: jackson@fusion.gat.com

Abstract. DIII-D experiments have investigated ITER startup scenarios, including an initial phase where the plasma was limited on low field side (LFS) poloidal bumper limiters. Both the original ITER "small-bore" (constant q_{95}) startup and a "large-bore" lower internal inductance (l_i) startup have been simulated. In addition, l_i feedback control has been tested with the goal of producing discharges at the ITER design value, $l_i(3)$ = 0.85. These discharges have been simulated using the Corsica free boundary equilibrium code. High performance hybrid scenario discharges (β_N = 2.8, $H_{98,y2}$ = 1.4) and ITER H-mode baseline discharges (β_N > 1.6, $H_{98,y2}$ = 1–1.2) have been obtained experimentally in an ITER similar shape after the ITER-relevant startup.

1. Introduction

ITER startup presents unique challenges due to the low inductive toroidal electric field (0.3 V/m), power supply and poloidal field coil constraints, and (in some scenarios) plasma current rampup near the $n = 0$ vertical stability limit. Important goals of this work are to test whether the proposed ITER startup scenarios are feasible, to benchmark modeling codes, and to develop improvements to these scenarios.

To simulate ITER startup in DIII-D, the limiter phase of the current ramp was scaled by the ratio of the low field side (LFS) radii of both devices, $R_{\mathrm{LFS,ITER}} / R_{\mathrm{LFS,DIII\text{-}D}} \approx$ 3.5. During the diverted phase, the scaling factor was set by the major radii and was 3.65. The DIII-D toroidal field, B_T, was 2.14 T at the major radius R = 1.7 m (compared to 5.3 T at R = 6.2 m in ITER). The scale factor to give the same relative times for the L / R_{plasma} time in DIII-D and ITER is about 50 (L and R_{plasma} are internal inductance and resistance, respectively). For similar I / aB, the original 15 MA ITER baseline rampup in 110 s scales to 1.7 MA in 2.2 s for DIII-D. For the large-bore ITER scenario, discussed below, a faster ramp is specified corresponding to 1.64 MA in 1.6 s in DIII-D. In DIII-D, there are three poloidal bumper limiters on the LFS, extending 2 cm from the surrounding graphite wall tiles.

In DIII-D, the original ITER startup baseline scenario has been investigated [1]. In this scenario [2], referred to here as the small-bore scenario, the discharge was initiated on the LFS limiters and plasma current was increased while edge q (q_{95}) was maintained approximately constant. The discharge was diverted at $q_{95} \approx 5.7$ at 0.6 s, corresponding to $I_p / aB_T \approx 0.71$ in ITER. During the Ohmic phase, the internal inductance $l_i(3)$ typically increased to 1.2 or higher sometimes leading to locked modes and disruptions. In this paper, in order to be consistent with ITER specifications, we will use a normalized internal inductance, $l_i(3)$, defined by

$$l_i(3) = 2V\left\langle B_p^2 \right\rangle \Big/ \left[\left(\mu_0 I_p\right)^2 R \right] \quad , \tag{1}$$

where B_p is the poloidal magnetic field, $\langle B_p^2 \rangle = 1/V \int B_p^2 \, dV$ and V is the plasma volume. An alternate startup scenario [3] has also been investigated in DIII-D, referred to as the large-bore scenario. In this scenario, the discharge is also initiated on the LFS, but diverted much earlier, $I_p / aB_T \approx 0.40$, and the plasma volume during the limited phase is larger. This scenario reduces heat flux to the LFS limiters and torus wall and has lower internal inductance. An example of the evolution of a large bore discharge is shown in Fig. 1 and

compared to that calculated for a similar evolution in ITER. As shown in Fig. 1, the higher plasma volume for the large-bore scenario allows more flexibility in locating the electron cyclotron (EC) resonance inside the last closed flux surface (LCFS) for effective auxiliary heating during early evolution, including the burnthrough phase. For the DIII-D experiments, second harmonic X-mode (X2) EC assist was evaluated during the time when the discharge was limited on the LFS. Two gyrotrons were used (DIII-D has six gyrotrons with a nominal source power of 1 MW each) with a launch angle normal to the toroidal field (perpendicular launch). The injected power was 1 to 1.3 MW. The vacuum resonance location for the fundamental O-mode (O1) of the ITER 170 GHz gyrotrons is shown in Fig. 1(a).

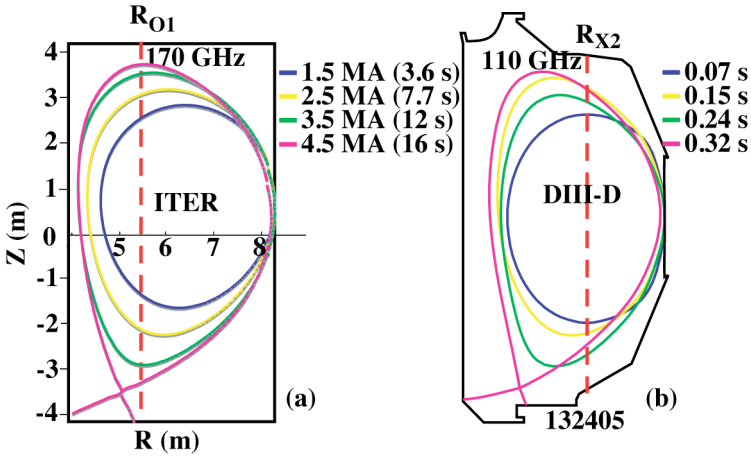

Fig. 1. Shape evolution for the large-bore LFS startup in ITER (a) and in the DIII-D scaled startup (b). ITER:DIII-D scaling is 3.5:1 (size) and 50:1 (time). The diverted shape is just after the end of the limited phase. The nominal resonance location of both EC systems is shown as dashed lines.

The ITER small-bore startup scenario is discussed in Ref. [1] and compared to the large-bore startup. In this paper, we will present results from experiments using the improved large-bore startup that has been extended to initiation at lower toroidal electric field and ramped to higher I_p. Section 2 discusses low voltage breakdown and flux consumption during current rampup, Section 3 presents experiments to control internal inductance, Section 4 gives examples of rampup using the ITER scenario leading to ITER baseline H-mode and Hybrid phases, Section 5 discusses benchmarking these large-bore discharges using the Corsica code, followed by conclusions in Section 6.

2. Low Voltage Startup and Flux Consumption

The ITER design assumes an applied toroidal electric field, E_ϕ, of 0.3 V/m during the breakdown phase. This field is limited by induced currents in the thick vacuum vessel and poloidal field coil constraints. Since most present day tokamaks operate at much higher values of E_ϕ, we refer to the reduced field as low voltage startup, where the toroidal loop voltage, $V_L = \int E_\phi \, dl$. The electric field produces ionization of the neutral gas and provides Ohmic heating power for the plasma during the breakdown and current rampup phases. If this Ohmic power is too low, then burnthrough of low Z impurities may not occur and startup will fail. Although ITER has been designed to allow Ohmic startup, ECH will provide additional power to facilitate the burnthrough phase. EC assist for both fundamental O-mode and second harmonic X-mode has been shown to be effective for pre-ionization and burnthrough in a variety of tokamaks [1,4–8]. Shown in Fig. 2 is the early evolution of two similar DIII-D discharges: one Ohmic, and one with EC assist. The additional power provided by electron cyclotron heating (ECH) results in a rapid current rise [Fig. 2(a)] and prompt burnthrough of low Z impurity charge states; an example of C^{III} is plotted in [Fig. 2(c)]. In both discharges, the current channel forms on the high field side (HFS) [Fig. 2(b)], but EC assist produces a more rapid current rise. That the EC power is effectively heating the discharge is shown in Fig. 2(d) and (f) where both electron temperature and plasma stored energy are higher for the ECH discharge. Although the fraction of radiated power is initially high with ECH, possibly due to low single-pass absorption, it rapidly decreases and is nearly equal to the ohmic case by 0.08 s. After the discharge diverts (not shown), there is virtually no difference in radiated power between these two cases.

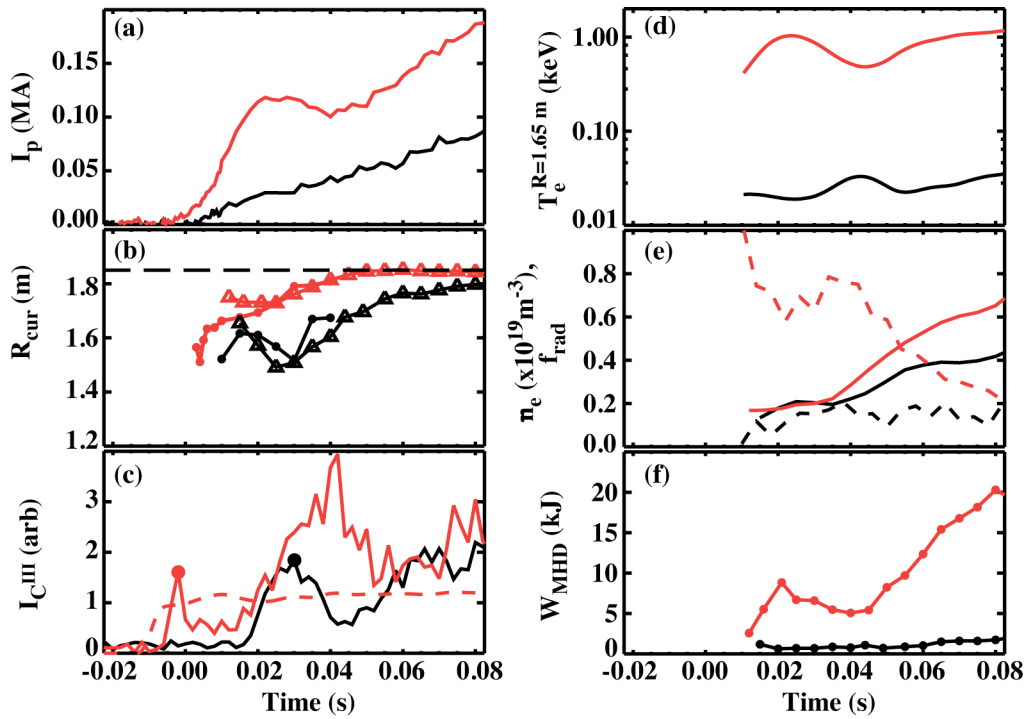

Fig. 2. Comparison of Ohmic (black) and EC assist (red) startup with E_ϕ = 0.43 V/m. Shown are: (a) plasma current, (b) radius of current centroid using EFIT (triangles) and a single filament fit (circles), (c) C^{III} intensity with circles indicating approximate burnthrough time, (d) electron temperature, (e) line average electron density (solid) and fraction of radiated power ($f_{rad} = P_{rad} / P_{in}$), and (f) plasma stored energy. The second harmonic EC resonance location is shown as a horizontal dashed line in (b).

The comparison in Fig. 2 is for two similar discharges with the initial electric field held constant at 0.43 V/m. This is the lowest voltage startup obtained Ohmically in these experiments using the LFS ITER large-bore scenario. Ohmic attempts at 0.3 V/m produced breakdown but not burnthrough. We note that previous work [4] demonstrated ohmic startup in DIII-D at 0.25 V/m limiting on the HFS. Future experiments will continue to explore ohmic LFS startup at or below 0.3 V/m to determine the fundamental physics constraints for inductive startup. Although *Ohmic* discharge initiation was not at sufficiently low E_ϕ for ITER, discharges with EC assist were successfully ramped to current flattop with electric fields as low as 0.21 V/m. In this scenario, ECH was applied during the LFS limiter phase. The breakdown and current initiation were prompt with ECH, and startup was robust. The inductive and resistive flux consumption, defined in Ref. [9], for three low voltage discharges is plotted in Fig. 3 as a function of I_p. In these similar discharges, the inductive flux is nearly identical, as expected. However there is a resistive flux reduction with the discharges using EC assist. The electric field during the limited phase is different for the lowest voltage discharge shown in green. During the divertor phase, the voltage driving the Ohmic field coil is programmed to produce a constant current ramp in all three cases and is approximately 0.22 V/m. The Ejima coefficient [9] shown in Fig. 3(b) is also lower using ECH although ECH was only on during the LFS limited phase up to 0.24 s, (current flattop occurred at 1.63 s). The Ejima coefficient, C_E, is an indication of the resistive flux consumption and is given by

$$C_E = \Delta\Phi_R / \mu_0 R I_p \quad , \tag{2}$$

where $\Delta\Phi_R$ is the resistive flux obtained by subtracting the plasma poloidal flux (calculated from EFIT) from the total flux at the plasma boundary [9,10]

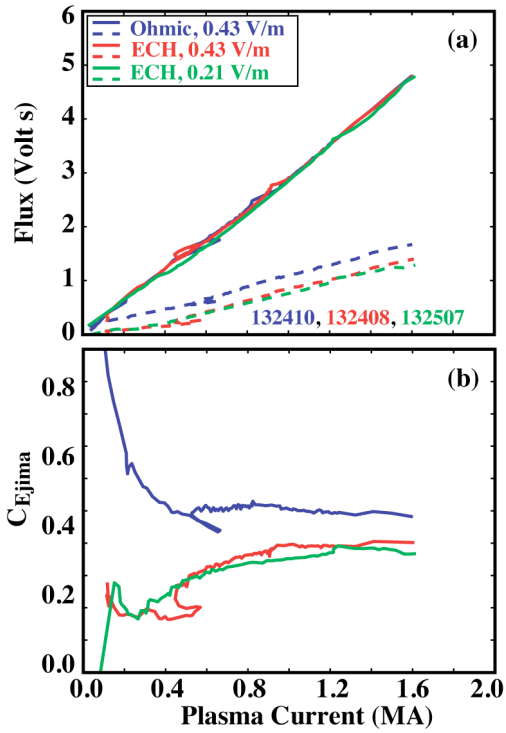

Fig. 3. (a) Inductive (solid) and resistive (dashed) flux consumption during the current ramp and (b) the Ejima coefficient for three similar discharges with 0.43 V/m (red and blue) and 0.21 V/m (green) startup.

As expected in Fig. 3, the higher temperatures with ECH [Fig. 2(d)] resulted in a lower Ejima coefficient and these discharges required somewhat lower flux to reach current flattop.

3. Control of Internal Inductance

Due to the thick ITER vacuum vessel and constraints on the poloidal field coils, ITER must reach 15 MA within a relatively narrow range of internal inductance around a nominal value of $l_i(3) = 0.85$. Controlling $l_i(3)$ to remain in this range requires modification of the current profile. Three actuators have been used in DIII-D startup experiments to modify the current profile: (1) the ohmic heating power supply (to change the I_p ramp rate), (2) gas injectors (to vary density and indirectly plasma temperature), and (3) neutral beam auxiliary heating (to directly vary plasma temperature). These will be discussed below.

Feedback control of $l_i(3)$ has been successfully demonstrated by varying the current ramp rate, as shown in Fig. 4. This feedback allows the flexibility to control l_i in a systematic way to avoid limitations in the ITER poloidal field coil set without prior knowledge of the exact evolution of the current profile. The current feedback algorithm has been described in Ref. [1] and the algorithm has recently been enhanced to allow feedback control using $l_i(3)$ as the target. The feedback circuit uses the DIII-D plasma control system (PCS) to perform a realtime equilibrium reconstruction [11] to calculate $l_i(3)$ and then generates an error signal to increase or decrease the current ramp rate by controlling the voltage of the actuator, i.e., the ohmic heating power supply. The range of $l_i(3)$ target values in Fig. 4 varies from 0.65 to 0.95. At the lowest value of $l_i(3)$ corresponding to the fastest current ramp, there is a locked mode near current flattop and eventually a disruption. All discharges were Ohmically ramped to flattop except the discharge with a target value of 0.75. In this discharge, neutral beam heating power was applied during the ramp at 1.6 s, and an H-mode phase ensued. The PCS feedback then limited the current to the minimum allowable ramp rate, but the $l_i(3)$ target value could not be maintained. In all discharges $l_i(3)$ feedback control was not maintained around the time of Ohmic supply current crossover, when a switching network changes the current polarity in the Ohmic field coils (the power supply is unipolar). This is seen as a sudden increase in $l_i(3)$ in Fig. 4 as I_p flattens prior to switching, and then a drop in $l_i(3)$ when the switch is reconnected and the ramp rate increases to catch up with the requested current. However feedback

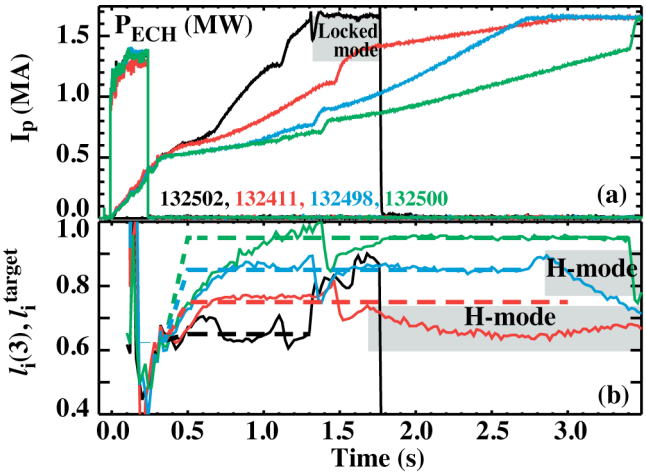

Fig. 4. Feedback control of internal inductance by varying the I_p ramp rate (a). The target values of $l_i(3)$ are shown as dashed lines during the time that feedback was enabled, (b). The value of $l_i(3)$ calculated in the PCS using rtEFIT is also shown in (b). Feedback is enabled at 0.35 s and ramped to the desired flattop value at 0.5 s, as described in Ref. [1].

is again effective in bringing $l_i(3)$ back to the target value. Except for the current crossover times, the feedback is effective for the entire current ramp for the two discharges at highest target values.

Another method of $l_i(3)$ modification is to change the current profile by using auxiliary heating. Shown in Fig. 5 is l_i feedback for four levels of neutral beam heating and an ohmic comparison (the means of heating is not critical; it is the change in conductivity that is important). Note that in this case, the PCS calculated l_i, and not $l_i(3)$ for feedback control [$l_i(3)$ feedback had not been implemented]. The effect of heating is shown indirectly by changes in the current ramp as the neutral beam power is increased while maintaining constant l_i with feedback.

The third method of internal inductance control is to modify the plasma density with external fueling. A limited scan has been reported in Ref. [1] for the small-bore scenario and was also tried for the large-bore discharges. In the latter case, while $l_i(3)$ could be increased with gas puffing, the highest density led to MARFES and this approach has not been investigated as extensively as the other two techniques described above.

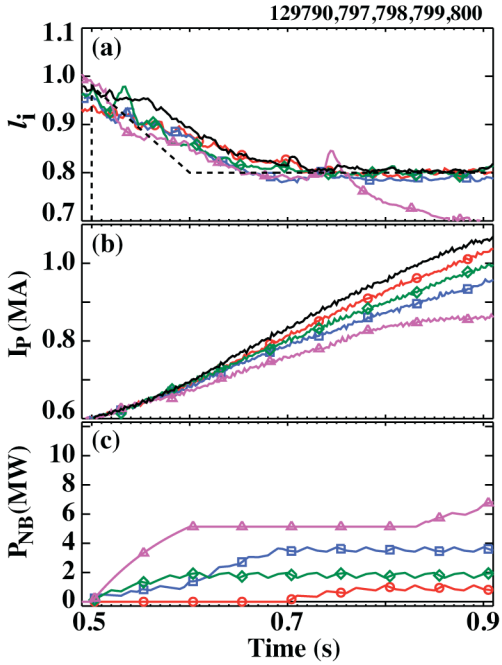

Fig. 5. Feedback control of internal inductance (a) for 5 large-bore discharges as neutral beam power is varied, (c). The current ramp rate, (b), decreases as power is increased to maintain the same target l_i of 0.8. Also shown (black) is an Ohmic discharge. There is an L-H transition at 0.73 s in highest power discharge (magenta) and l_i feedback can no longer maintain the target value, going to the minimum allowable current ramp determined by the feedback algorithm.

4. Achieving ITER Flattop Scenarios with Large-Bore Startup

The entire ITER rampup scenario has been simulated in DIII-D, beginning with a large-bore, low voltage (0.29 V/m), LFS limited startup with EC assist and then ramping the current in the approximate ITER divertor shape to the flattop phase. In other experiments, DIII-D has simulated the ITER shape during the flattop phase and demonstrated four ITER scenarios [12]. The work presented here shows that an ITER startup scenario can be combined with some of these ITER flattop scenarios. A typical discharge is shown in Fig. 6, where the flattop parameters are $q_{95} = 3.0$, $I/aB = 1.39$. After auxiliary heating is applied, an H-mode phase is observed ($H_{98,y2} \approx$ 1–1.2, $H_{89} \approx$ 1.6–2.3, and $\beta_N > 1.6$), simulating the ITER 15 MA $Q = 10$ H-mode scenario 2 ($I/aB = 1.42$, $\beta_N \approx$ 1.8, $H_{89} \approx$ 2). With 1 MW of ECH, breakdown and burnthrough were robust for all discharges in this series. While not the main subject of this paper, we note in passing that this discharge was successfully ramped down, limiting on the HFS at $I_p = 0.33$ MA (not shown). However, the rampdown phase required auxiliary heating to remain in H-mode and had a rather high $l_i(3)$ [Fig. 6(d)] that would probably not be possible in ITER. Further work is required for the ITER rampdown phase.

The ITER large-bore startup has also been used to produce a high performance hybrid scenario discharge, shown in Fig. 7. In this case a 12 MA ITER hybrid discharge was simulated with a figure of merit, $G = \beta_N \times H_{89P}/q_{95}^2 = 0.40$, [Fig. 7(d)], approaching the value required in ITER, $G = 0.42$, for a fusion gain $Q = 10$. The discharge was ramped to $q_{95} = 4.2$ using the large- bore Ohmic startup. Only short neutral beam pulses were used during this period for diagnostic purposes. After applying 6.6 MW of neutral beam power, plasma current was ramped slightly to maintain q_{95} as plasma stored energy increased during the hybrid phase, then neutral beam feedback was used to maintain $\beta_N \approx 2.8$. Small Ohmic

sawteeth were observed late in the current ramp, but these were suppressed with auxiliary heating and during the hybrid phase $q_{\min}$ was generally above unity.

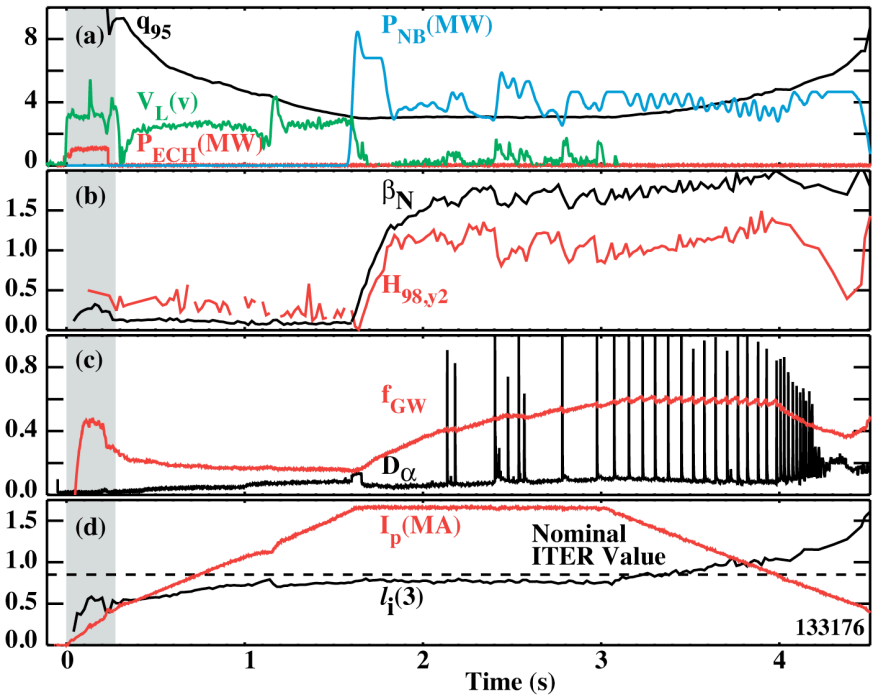

Fig. 6. DIII-D discharge simulating ITER scenario 2 and using a low voltage large-bore startup with ECH assist (a). Shaded area indicates LFS limited phase. Plotted are: (a) q_{95}, toroidal loop voltage (V_L), neutral beam power, and ECH power; (b) normalized beta (β_N) and the H factor; (c) D_α intensity and the Greenwald fraction; and (d) plasma current and $l_i(3)$.

5. Modeling of ITER Startup Scenario

In order to make model-based predictions for ITER startup, the analysis codes must be benchmarked against experimental data. For DIII-D, the electron thermal transport model in the Corsica code is being benchmarked using the both small-bore and large-bore discharges.

Corsica [13] is a free-boundary equilibrium and transport code that can model both DIII-D and ITER scenarios [14]. It evolves the plasma shape and plasma parameters such as l_i, $j(\psi)$, and T_e and provides capability for modeling shape and vertical stability controllers and active feedback control systems. Transport calculations have been implemented using a gyro-Bohm based thermal transport model [15]. Figure 8 is an example of a simulation comparing the temporal evolution of $T_e(0)$, q_0, and internal inductance from Corsica with EFIT. For this Corsica simulation, the measured electron density is input at each time step and impurity density is fixed at

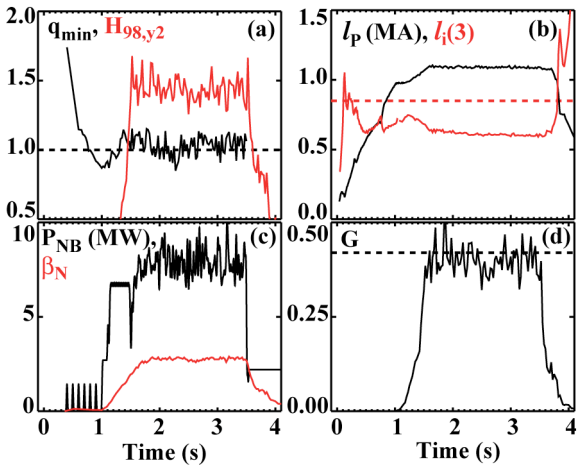

Fig. 7. ITER large-bore startup scenario and ITER similarity shape in a high performance Hybrid discharge: (a) $q_{\min}$ and H factor, $H_{98,y2}$, (b) I_p and $l_i(3)$, (c) auxiliary heating power and β_N, and (d) G factor. ITER nominal design value, $l_i(3) = 0.85$ is shown as a dashed line in (b) and calculated value of G to produce a fusion gain, $Q = 10$ is a dashed line in (d).

$n_{carbon}/n_e = 0.03$. This initial modeling predicts the approximate time of sawteeth onset ($q_{\min} = 1$) and reproduces the electron temperature evolution during the startup phase. With the same model and parameter values as used for ITER predictions, the evolved on-axis electron temperature prediction obtained, Fig. 8(b), is in reasonably good agreement with that obtained from profile fits to Thomson scattering measurements. Similarly good agreement for the temperature profile is also indicated in Fig. 8(b) [inset] at 0.75 s into the discharge. In Fig. 8(c), we compare the on-axis safety factor, q_0, obtained from the current profile evolution in simulations with that obtained from EFIT analysis. Since the ITER prescription for startup does not include auxiliary heating in the current ramp, there is no neutral beam heating in the current ramp for these experiments. However, we have a single short beam pulse at 0.35 s for diagnostic measurements, notably the MSE measurement needed for accurate prediction of q_0. We show the MSE-constrained evaluation of q_0 at this time in Fig. 8(c) and note that it is in reasonably good agreement with the simulated evolution of q_0. We also show that the onset of sawtooth activity [Fig. 8(b)], observed by a central channel of the electron cyclotron emission (ECE) diagnostic, corresponds approximately to the time the simulated $q_0 \sim 1$, further indicating that the predicted current profile evolution is consistent with the experiment. This is important since stability is linked to the evolution of the internal inductance and l_i values higher than ITER design limits must be carefully considered. We show in Fig. 8(d), the comparison of predicted $l_i(3)$ from simulations with that obtained from the EFIT analysis optimized for startup conditions and note that there is a discrepancy between the predicted and simulated values during the ramp. This is due to some differences in the current profile structure between simulation and experiment. We are continuing our analysis and modeling to resolve the source of this difference and to further improve the accuracy of the modeling.

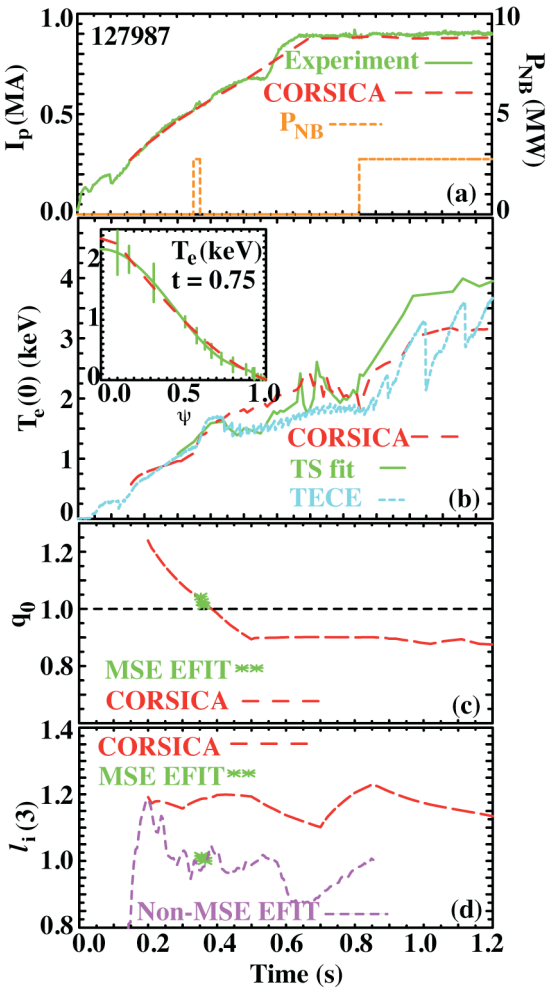

Fig. 8. Corsica modeling of a DIII-D small-bore scenario discharge comparing (a) measured and modeled I_p, (b) measured central electron temperature (ECE and Thomson scattering) and model calculation, (c) Corsica and EFIT calculations of q_0, and (d) Corsica and EFIT calculations of $l_i(3)$. EFIT calculations with the MSE diagnostic to determine q_0 are only available during times with neutral beam injection (a).

6. Conclusions

The large-bore startup scenario with EC assist has proven to be robust at ITER relevant toroidal electric fields, as low as 0.21 V/m. With ECH, the time of plasma initiation is reproducible which may be an important consideration for ITER. Ohmic LFS startup with $E_\phi = 0.43$ V/m has also been obtained. LFS startup experiments at lower E_ϕ without EC assist have not yet achieved burnthrough, although there appears to be no fundamental factors that would exclude this. However, it is clear from this work that the operating parameter range for Ohmic startup is more limited than for startup with EC assist. EC assist can also

lower the resistive flux required to ramp to flattop. In these experiments, the ECH was only applied during the LFS limited phase, however auxiliary heating during the entire rampup phase may provide additional flux reduction.

Feedback control of internal inductance has been demonstrated, allowing additional flexibility in control of the current profile, access to advanced scenarios, and avoidance of operational limits. In addition, the modification of internal inductance using neutral beam heating and gas puffing has been demonstrated, although feedback control using these actuators has not been done. We note that a combination of auxiliary heating, either neutral beam or ECH, and current ramp control might be used for ITER, providing l_i feedback and reducing the resistive flux consumption.

Although the work presented in this paper has focused on startup, it has also been extended to simulate the ITER rampdown phase. In initial experiments, a beam heated H-mode rampdown phase has been successfully produced.

The DIII-D experiments simulating ITER startup have shown that plasma current can be initiated while limited on the LFS, diverted early in time to minimize heat flux to the outer wall, and ramped to values of I/aB comparable to the ITER 15 MA scenario. Using this large-bore startup, both the ITER H-mode baseline scenario and an advanced inductive hybrid mode (ITER scenario 3) have been successfully demonstrated.

Acknowledgment

This work supported by the U.S. Department of Energy under DE-FC02-04ER54698 and DE-AC52-07NA27344. This report was prepared as an account of work by or for the ITER Organization. The Members of the Organization are the People's Republic of China, the European Atomic Energy Community, the Republic of India, Japan, the Republic of Korea, the Russian Federation, and the United States of America. The views and opinions expressed herein do not necessarily reflect those of the Members or any agency thereof.

References

[1] JACKSON, G.L, et al., "ITER startup studies in the DIII-D tokamak," submitted to Nucl. Fusion (2008).
[2] GRIBOV, Y., HUMPHREYS, D., KAJIWARA, K., LAZARUS, E.A., LISTER, J.B., OZEKI, T., PORTONE, A., SHIMADA, M., SIPS, A.C.C., WESLEY, J.C., Nucl. Fusion **47**, S385 (2007).
[3] LUKASH, V.E., KAVIN, A.A., KHAYRUTDINOV, R.R., GRIBOV, Y.V., MINEEV, A.B., Study of early phase of current ramp-up in ITER with DINA code, 35th EPS Plasma Phys. Conf., Hersonissos, Crete, Greece, 2008.
[4] LLOYD, B., et al. Nucl. Fusion **31**, 2031 (1991).
[5] JACKSON, G.L., et al. Nucl. Fusion **47**, 2007 (257).
[6] ERCKMANN, V., GASPARINO, U., Plasma Phys. Control. Fusion **36**, 1869 (1994).
[7] KAJIWARA, K., IKEDA, Y., SEKI, M., MORIYAMA, S., OIKAWA, T., FUJII, T. and JT-60 TEAM, Nucl. Fusion **45**, 694 (2005).
[8] BUCALOSSI, J., HERTOUT, P., LENNHOLM, M., SAINT-LAURENT, F., BOUQUEY, F., DARBOS, C., TRAISNEL, E., TRIER, E., Nucl. Fusion **48**, 054005 (2008).
[9] MENARD, J.E., LeBLANC, B.P., SABBAGH, S.A., et al., Nucl. Fusion **41**, 1197 (2001).
[10] EJIMA, S., CALLIS, R.W., LUXON, J.L., et al., Nucl. Fusion **22**, 1313 (1980).
[11] FERRON, J.R., WALKER, M.L., LAO, L.L., St. JOHN, H.E., HUMPHREYS, D.A., LEUER, J.A., Nucl. Fusion **38** 1055 (1998).
[12] DOYLE, E.J., et al., these proceedings, EX/1-3.
[13] CROTINGER, J.A., et al., LLNL Report UCRL-ID-126284 available from NTIS #PB2005-102154 (1997).
[14] CASPER, T.A., JONG, R.A., MEYER, W.H., MOLLER, J.M., Fusion Engin. Design **83**, 552 (2008).
[15] JARDIN, S.C., BELL, M.G., POMPHREY, N., Nucl. Fusion **33**, 371 (1993).